


# Well defined phase boundaries and superconductivity with high Tc in PbSe single crystal

Jiawei Hu(胡佳玮), Yanghao Meng(孟养浩), He Zhang(张赫), Wei Zhong(钟韦), Hang Zhai(翟航), Xiaohui Yu(于晓辉), Binbin Yue(岳彬彬), and Fang Hong(洪芳)

**Citation:**Chin. Phys. B, 2025, 34 (**4**): 046102. DOI: 10.1088/1674-1056/adb272
Journal homepage: http://cpb.iphy.ac.cn; http://iopscience.iop.org/cpb

**What follows is a list of articles you may be interested in**

---

## Pressure-induced stable structures and physical properties of Sr-Ge system

Shuai Han(韩帅), Shuai Duan(段帅), Yun-Xian Liu(刘云仙), Chao Wang(王超), Xin Chen(陈欣), Hai-Rui Sun(孙海瑞), and Xiao-Bing Liu(刘晓兵)
Chin. Phys. B, 2023, 32 (**1**): 016101. DOI: 10.1088/1674-1056/ac6db5

## Structural evolution and molecular dissociation of $H_2S$ under high pressures

Wen-Ji Shen(沈文吉), Tian-Xiao Liang(梁天笑), Zhao Liu(刘召), Xin Wang(王鑫), De-Fang Duan(段德芳), Hong-Yu Yu(于洪雨), and Tian Cui(崔田)
Chin. Phys. B, 2022, 31 (**7**): 076102. DOI: 10.1088/1674-1056/ac5980

## Structural modulation and physical properties of cobalt-doped layered $La_2M_5As_3O_2$ (*M*= Cu, Ni) compounds

Lei Yang(杨蕾), Yan-Peng Song(宋艳鹏), Jun-Jie Wang(王俊杰), Xu Chen(陈旭), Hui-Jing Du(杜会静), and Jian-Gang Guo(郭建刚)
Chin. Phys. B, 2021, 30 (**7**): 076106. DOI: 10.1088/1674-1056/abf349

## Low temperature *Pmmm* and *C*2/*m* phases in $Sr_2CuO_{3+\delta}$ high temperature superconductor

Hai-Bo Wang(王海波), Zhen-Lin Luo(罗震林), Yuan-Jun Yang(杨远俊), Qing-Qing Liu(刘清青), Si-Xia Hu(胡思侠), Meng-Meng Yang(杨蒙蒙), Chang-Qing Jin(靳常青), Chen Gao(高琛)
Chin. Phys. B, 2019, 28 (**5**): 056103. DOI: 10.1088/1674-1056/28/5/056103

## Stability of concentration-related self-interstitial atoms in fusion material tungsten

Hong Zhang(张红), Shu-Long Wen(温述龙), Min Pan(潘敏), Zheng Huang(黄整), Yong Zhao(赵勇), Xiang Liu(刘翔), Ji-Ming Chen(谌继明)
Chin. Phys. B, 2016, 25 (**5**): 056102. DOI: 10.1088/1674-1056/25/5/056102

---

**SPECIAL TOPIC — Structures and properties of materials under high pressure**

# Well defined phase boundaries and superconductivity with high $T_c$ in PbSe single crystal

Jiawei Hu(胡佳玮)[1,2,3,†], Yanghao Meng(孟养浩)[3,4,†], He Zhang(张赫)[3,4], Wei Zhong(钟韦)[5], Hang Zhai(翟航)[3,6], Xiaohui Yu(于晓辉)[3,4,7,‡], Binbin Yue(岳彬彬)[5,§], and Fang Hong(洪芳)[3,4,7,¶]

[1] *Key Laboratory of Materials Physics, Institute of Solid State Physics, HFIPS, Chinese Academy of Sciences, Hefei* 230031, *China*
[2] *University of Science and Technology of China, Hefei* 230026, *China*
[3] *Beijing National Laboratory for Condensed Matter Physics, Institute of Physics, Chinese Academy of Sciences, Beijing* 100190, *China*
[4] *School of Physical Sciences, University of Chinese Academy of Sciences, Beijing* 100190, *China*
[5] *Center for High Pressure Science and Technology Advanced Research, Beijing* 100094, *China*
[6] *State Key Laboratory of Superhard Materials, International Center for Computational Method and Software, and Jilin Provincial International Cooperation Key Laboratory of High-Efficiency Clean Energy Materials, Jilin University, Changchun* 130012, *China*
[7] *Songshan Lake Materials Laboratory, Dongguan* 523808, *China*

(Received 10 January 2025; revised manuscript received 3 February 2025; accepted manuscript online 5 February 2025)

Lead chalcogenides represent a significant class of materials that exhibit intriguing physical phenomena, including remarkable thermoelectric properties and superconductivity. In this study, we present a comprehensive investigation on the superconductivity of PbSe single crystal under high pressure. The signature of superconducting (SC) transition starts to appear at 7.2 K under 16.5 GPa. Upon further compression, the SC temperature ($T_c$) decreases, and it is reduced to 3.5 K at 45.0 GPa. The negative pressure dependent behavior of $T_c$ is consistent with the trend of $T_c$–$P$ relations observed in other lead chalcogenides. The highest $T_c$ is 8.0 K observed at 20.5 GPa during decompression process, which is also the highest record among all other PbSe derivatives, such as doped samples, superlattices, and so on. The phase boundaries of the structural and electronic transitions are well defined by Raman spectroscopy, and then phase diagrams are plotted for both compression and decompression processes. This work corrects the previous claim of positive pressure dependence of $T_c$ in PbSe and provides clear phase diagrams for intrinsic superconductivity in PbSe under pressure.

**Keywords:** superconductivity, high-pressure electrical transport, Raman spectroscopy, phase diagrams

**PACS:** 61.50.Ks, 74.62.Fj, 73.61.–r, 74.25.nd, 74.25.Dw

**DOI:** 10.1088/1674-1056/adb272 **CSTR:** 32038.14.CPB.adb272

## 1. Introduction

Lead chalcogenide compounds, specifically Pb$X$ (where $X$ represents S, Se, or Te), are well-known as good thermoelectric materials.[1–4] Lead chalcogenides have small direct band gaps $E_g$ of 0.2–0.41 eV located at the $L$ point of the Brillouin zone[5,6] which can be tuned easily by doping,[7] alloying,[8] lowering dimension[9] and heterostructures.[10] This feature may cause band inversions at the $L$ point, which leads to a non-trivial topological state, making them promising candidates as topological crystalline insulators.[7,9–13] Superconductivity can also be induced in lead chalcogenides through doping,[14] heterostructures,[15] and superlattices.[16] The equivalent pressure effects such as strain-induced effect[17] and edge misfit dislocations[15,16,18] play a key role in their superconductivity. In the past several decades, there were lots of works about the pressure effect on the structural and electrical properties of lead chalcogenides, which help to explain the superconductivity observed in Pb$X$-based systems at ambient pressure. Under ambient conditions, lead chalcogenides are in the form of a NaCl-type structure (B1 phase).[5,6] As pressure is applied, the crystal structures undergo one or two discrete phase transitions (intermediate phase),[19,20] at which the band gaps become significantly larger. After that, the high-pressure CsCl-type structure emerges,[21–29] refered to as B2 phase. In the B2 phase, lead chalcogenides become metals and superconductors. In PbS, PbSe, and PbTe, their highest SC $T_c$ values are 12.3 K,[30] 6.7 K[31] and 8.0 K,[31] respectively.

The earlier study on the superconductivity in compressed PbSe was conducted in 1975,[31] finding that the superconductivity occurs above 30 GPa, and PbSe exhibits a positive pressure dependence of $T_c$ that $T_c$ increases with increasing pressure. However, in the same work, $T_c$ values of PbTe show a negative pressure dependence. Recently, a negative pressure dependent $T_c$ trend is also observed in B2 phase of PbS.[30]

[†]These authors contributed equally to this work.
[‡]Corresponding author. E-mail: yuxh@iphy.ac.cn
[§]Corresponding author. E-mail: yuebb@hpstar.ac.cn
[¶]Corresponding author. E-mail: hongfang@iphy.ac.cn

© 2025 Chinese Physical Society and IOP Publishing Ltd. All rights, including for text and data mining, AI training, and similar technologies, are reserved.

Considering the similarity among PbS, PbSe, and PbTe, the positive pressure dependence trend of $T_c$ in PbSe[31] looks very strange and may not make sense: they undergo similar structural phase transitions under pressure, and Se locates in the middle between S and Te on the periodic table. In addition, there are also reports on the doped PbSe[32] and doped PbTe,[33] and the $T_c$ values in both of them show a negative pressure dependence. Hence, to clarify this conflict, it is necessary to reevaluate the superconductivity in PbSe under pressure.

In this study, we conducted high-pressure electrical transport and Raman spectroscopy experiments on a PbSe single crystal. Superconductivity was found to initiate at a pressure as low as 16.5 GPa with a $T_c$ of 7.2 K and was suppressed upon further compression. This finding differs from a previous work which reported that the SC transition in PbSe starts from 30 GPa.[31] Signatures of multiband superconductivity behavior were observed, resembling its sister compound PbS.[30] Additionally, the highest $T_c$ of 8.0 K was observed at 20.5 GPa during the decompression process. By combining electrical transport results with Raman spectroscopy data, we present a phase diagram of PbSe under pressure and correct the previously reported superconductivity behavior of PbSe.[31] The intrinsic superconductivity of PbSe shows the highest $T_c = 8.0$ K among other derivatives like doped samples, nanocrystal films, heterostructures and superlattices as shown in Fig. 1.[15,34–37]

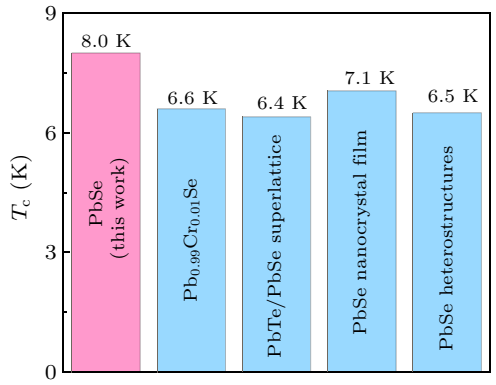



**Fig. 1.** Comparison of highest $T_c$ among PbSe and its derivatives.

## 2. Experimental details

The PbSe single crystal was synthesized by the chemical vapor transport method. High-purity Pb and Se powders were mixed in a 1:1 stoichiometric ratio and placed in a quartz tube under high vacuum. The tube was heated to 850 °C on one side, causing the powder mixture to vaporize, and the single crystal was formed at 500 °C on the other side. No transport agent was used in the CVT process.

We measured the temperature-dependent electrical resistance of the PbSe single crystal under high pressure with standard four-probe geometry.[30,38–40] We pressed the rhenium gasket with diamonds and drilled a hole in the center with a diameter of 200 μm. The culet sizes of our diamonds in this experiment are 300 μm. Then we filled the chamber with mixture of c-BN and epoxy. After that, we re-drilled a hole with a diameter of 100 μm in the center as the sample chamber. A small piece of the thin rectangular PbSe flake was loaded into the sample chamber. Four Pt electrodes were placed on the sample's surface. The voltage leads are in contact with the PbSe inside the sample chamber. We used KBr as the pressure medium. A ruby ball was placed near the sample to calibrate pressure.[41] The measurement was performed in a commercial cryostat (Janis Research) in the temperature range from 1.7 K to 300 K by a Keithley 6221 current source and a 2182A nanovoltmeter.

High pressure Raman spectra were collected on a HORIBA Raman spectroscopy system equipped with a second-harmonic Nd:YAG laser. KBr was also used as the pressure medium. A 532-nm laser with a 12 μm spot size was employed. We used low fluorescent diamonds for the Raman measurement and calibrated pressure with a ruby ball.

## 3. Results and discussion

The electrical transport behavior of PbSe single crystal under pressure is presented in Fig. 2. Metallic-like behavior was observed at pressures below 1.8 GPa (as seen in the inset in Fig. 2(a)), which was consistent with previous report.[42] Upon compression to 3.5 GPa, clear semiconducting transport behavior emerged. The resistance was very large at low temperatures that it exceeded the range of the experimental apparatus. This critical pressure aligned with previous structural and electrical studies, where a phase transition occurs from the low-pressure B1 phase to an intermediate *Pnma* structure, resulting in semiconducting behavior with a wider band gap.[19,20] The semiconducting behavior persisted until 16.5 GPa. The resistance decreased monotonously when pressure increased from 3.5 GPa to 16.5 GPa. In contrast to a recent study[43] that identified a notable anomalous peak at approximately 250 K at low pressure. Their results also show an increase in resistance and semiconducting properties above 3.5 GPa. Our high-pressure resistance–temperature ($R$–$T$) curves align with their findings. Furthermore, the electrical transport measurements in this study are consistent with those reported in PbS[30] and PbTe[33] under pressure. The unexpected feature may be due to impurities in the sample.

At 16.5 GPa, a sudden resistance drop was observed around 7.2 K, suggesting the occurrence of SC transition, as shown in Fig. 2(b). Subsequently, the sample showed a state of zero resistance, and the SC transition became much sharper. The SC critical pressure near 16.5 GPa corresponds to the pressure where the B2 phase transition takes place.[21,28] The $T_c$ decreased with pressure, and such a trend is consistent with those in other lead chalcogenides.[30–33] Here we define $T_c$

as illustrated in Fig. 2(b), which is in the same way as other PbSe derivatives[15,34–37] and lead chalcogenides[30,32,33] articles. Superconductivity persisted in our transport experiment up to the maximum pressure of 45.0 GPa, at which it showed a $T_c$ of 3.5 K.

The transport behavior of PbSe during decompression process is shown in Figs. 2(c) and 2(d). It is noted that the critical temperature ($T_c$) increased initially as the pressure was reduced from 45.0 GPa, and the $T_c$ reached the maximum 8.0 K at 20.5 GPa. Then, $T_c$ began to decrease, and the sample went back to the semiconducting state below 11.0 GPa, as shown in Fig. 2(d).

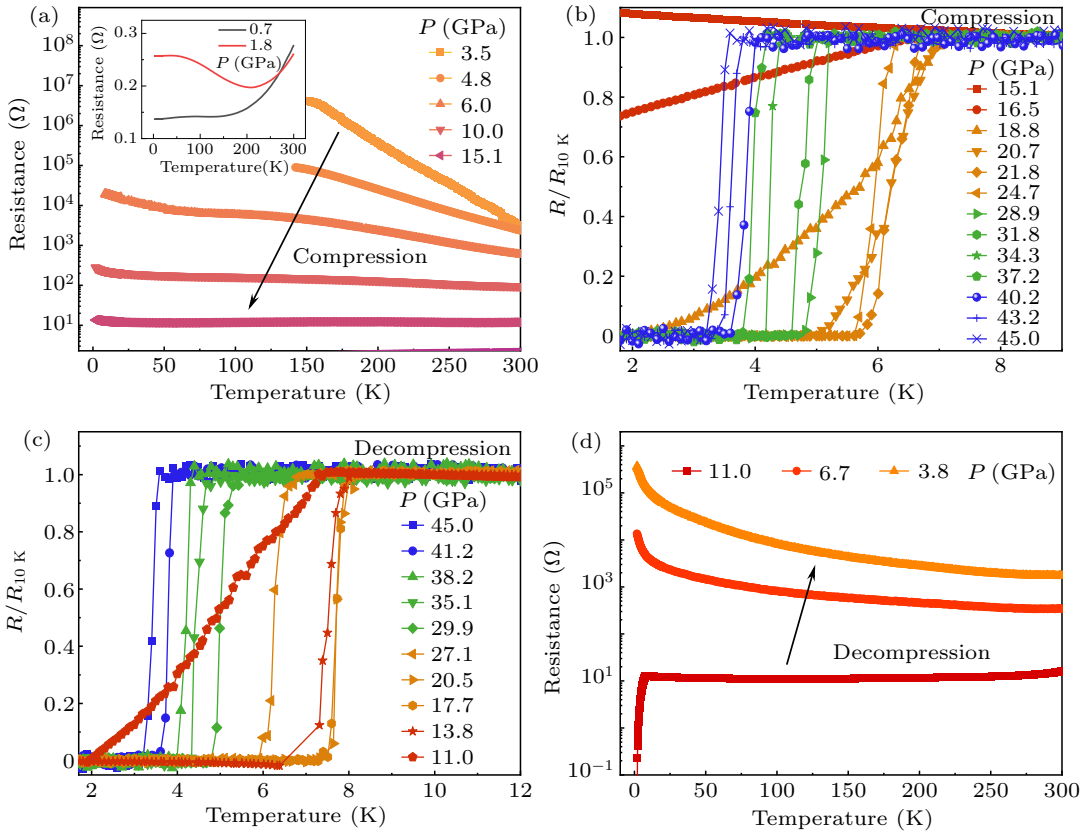



**Fig. 2.** The electrical transport behavior of PbSe single crystal under compression and decompression. (a) The *R*–*T* curves of PbSe from 3.5 GPa to 16.5 GPa upon compression. The inset shows the metal-like behavior near ambient pressure. (b) Normalized *R*–*T* curve of PbSe from 16.5 GPa to 45.0 GPa upon compression. (c) Normalized *R*–*T* curves of PbSe from 45.0 GPa to 11.0 GPa during decompression process. (d) *R*–*T* curves of PbSe from 11.0 GPa to 3.8 GPa during decompression.

Figure 3 shows the relation between $T_c$ and pressure in various lead chalcogenides in the B2 phase, and the corresponding pressure derivative $dT_c/dP$ values are listed in Table 1. For pure PbS, PbSe, and PbTe, they have similar $dT_c/dP$ values. However, the amplitudes of $dT_c/dP$ of PbSe ($-0.14$) and PbTe ($-0.19$) are 3–4 times larger than those of their doped derivatives ($-0.04$ and $-0.05$), suggesting that doping would help to stabilize the superconductivity. It is obvious that the $dT_c/dP$ of PbSe in this work has a different sign from $dT_c/dP$ of PbSe in Ref. [31]. We argue that the intrinsic superconductivity of PbSe has a negative pressure dependence. Because the SC transition pressures for PbS and PbTe correspond to the critical pressures of intermediate–B2 transition,[26,27,29–31] and our SC transition pressure coincides with the B2 transition pressure as well, as illustrated in Table 1. It is reasonable to believe that SC transition of PbSe should also emerge along with B2 phase, since Se lies in the middle of S and Te in the periodic table.

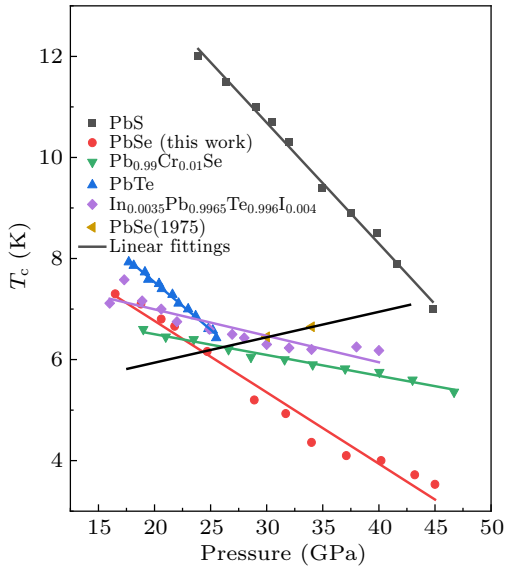



**Fig. 3.** The $T_c$–pressure diagram of lead chalcogenides in the B2 phase. The data of PbS is from Ref. [30], PbSe is from this work, PbTe is from Ref. [31], $Pb_{0.99}Cr_{0.01}Se$ is from Ref. [32] and $In_{0.0035}Pb_{0.9965}Te_{0.996}I_{0.04}$ is from Ref. [33]. Data are fitted linearly, shown in Table 1.

**Table 1.** Comparison of B2 transition pressures $P_{B2}$, SC onset pressure $P_{SC}$ and $dT_c/dP$ of lead chalcogenides in the B2 phase.

| Material | $P_{B2}$ (GPa) | $P_{SC}$ (GPa) | $dT_c/dP$ (K/GPa) |
|---|---|---|---|
| PbS | 21.1[c] | 23.9[d] | –0.24 |
| PbSe (this work) | 16[a] | 16.5 | –0.14 |
| PbTe | 18[b] | 17.5[e] | –0.19 |
| $Pb_{0.99}Cr_{0.01}Se$ | 20.1[f] | 19[f] | –0.04 |
| $In_{0.0035}Pb_{0.9965}Te_{0.996}I_{0.04}$ | 20.2[g] | 15.8[g] | –0.05 |
| PbSe (1975) | 16[a] | 30[e] | 0.05 |

[a]Ref. [21], [b]Ref. [27], [c]Ref. [29], [d]Ref. [30], [e]Ref. [31], [f]Ref. [32], [g]Ref. [33].

The effect of a magnetic field provides additional evidence of superconductivity, as illustrated in Fig. 4(a). At 28.9 GPa, the $T_c^{onset}$ was about 5.5 K (as indicated by the arrow). When an external magnetic field was applied, it suppressed the superconductivity, resulting in the decrease of SC temperature and broadening of the SC transition region.

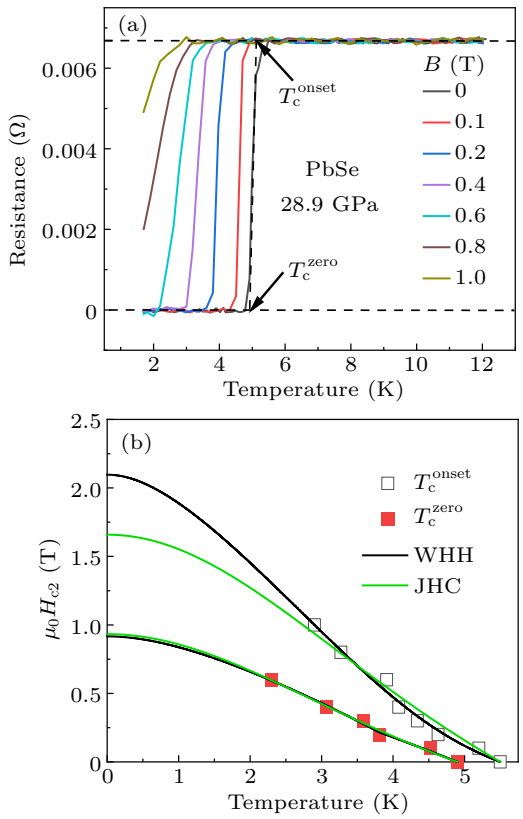



**Fig. 4.** Magnetic field effect on the superconductivity of PbSe and upper critical field analysis at 28.9 GPa. (a) The *R*–*T* curve of PbSe at 28.9 GPa under different magnetic fields. We extract $T_c^{onset}$ and $T_c^{zero}$ as illustrated by the arrows. (b) The upper critical field $H_{c2}$ as a function of temperature. The solid lines are the fitting results using the WHH and JHC formula.

Multiband superconducting behavior was observed through the evolution of $T_c$ under magnetic fields. We extracted $T_c$ by two different definitions, as illustrated in Fig. 4(a) for $T_c^{onset}$ and $T_c^{zero}$, then fitted the upper critical field $H_{c2}(T)$ with the two-band Werthamer–Helfand–Hohenberg (WHH) formula[44] which describes the $T_c$ dependence on magnetic field for multiband SC, as shown in Fig. 4(b). The corresponding $H_{c2}(0)$ values are 2.15 T for $T_c^{onset}$ and 0.9 T for $T_c^{zero}$. We also fitted $H_{c2}$ with Ginzburg–Landau (GL) theory. The fitted $H_{c2}(0)$ are 1.68 T and 0.93 T for $T_c^{onset}$ and $T_c^{zero}$, respectively. However, the fitted results for $T_c^{onset}$ obviously deviated from the measured results comparing to the WHH model, indicating the multiband SC nature in PbSe. It is worth mentioning that a similar multiband superconducting feature was also observed in its sister compound, PbS.[30] This finding suggests that the entire lead chalcogenide family may be characterized as multiband superconductors, a possibility that warrants further investigation.

To identify the distinct phase boundaries, we conducted Raman spectroscopy experiments on PbSe. Figure 5 displays the Raman spectra of PbSe during both compression (Fig. 5(a)) and decompression (Fig. 5(b)) processes. When pressures were below 4.8 GPa in the compression process, no significant Raman peak was observed, consistent with prior findings that the B1 phase of PbSe is not Raman active.[45] Clear peaks emerged above 4.8 GPa, confirming the transition from the B1 phase to the intermediate phase.[19,20,23,28] As the pressure was further increased, Raman peaks became more obvious, and they were kept up to 30.5 GPa, suggesting that the intermediate phase persisted until 30.5 GPa. Four clear Raman peaks were observed as shown in Fig. 5(c), recognized as three $A_g$ modes and one $B_{3g}$ mode respectively under *Pnma* symmetry (see supplemental material Table S1). Combining the results of transport and Raman measurements, it is believed that there is a mixed phase region composed of intermediate *Pnma* phase and B2 phase. It is reasonable given that this is a first-order transition.[23] Previous structural studies also purposed that the intermediate phase still persists after the emergence of B2 phase until near 30.0 GPa.[28] In order to check the structure stability at low temperature, we also conducted low temperature Raman spectra at 10.5 GPa and 20.0 GPa as shown in supplemental material Figs. S1(a) and S1(b). No new peak appeared, and no peak disappeared as we lowering the temperature, indicating no phase transition occurred in the temperature decreasing process. Above 30.5 GPa, the Raman signal became almost invisible, indicating that the intermediate phase fully transformed to the B2 phase.

During decompression process, the pure B2 phase was kept until 18.6 GPa, as shown in Fig. 5(b), below which the Raman signal of intermediate phase reappeared. Such a transition is almost consistent with the observation of the highest $T_c$ at 20.5 GPa during the decompression process, as shown in Fig. 2(d). When the pressure was released to 1.6 GPa and 1.0 GPa, the Raman signal decayed quickly, suggesting the phase transition to the original B1 phase.

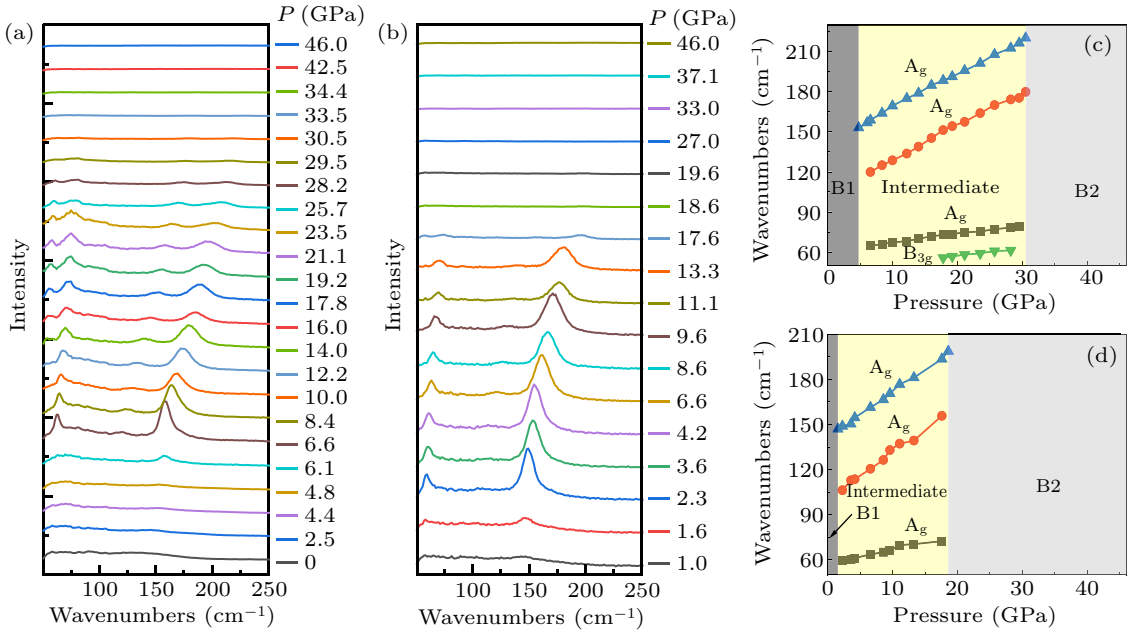



**Fig. 5.** Raman spectra of PbSe under high pressure. (a) Raman spectra of PbSe under compression. Clear Raman peaks started to appear above 4.8 GPa, indicating a phase transition from the B1 phase to the intermediate phase. Raman peaks did not vanish at 16.5 GPa but at 30.5 GPa, indicating a mixed phase of B2 phase and intermediate phase in this range.[30,32] (b) Raman spectra of PbSe under decompression. Raman peaks reemerged below 18.6 GPa. PbSe entered into the mixed phase. Below 1.6 GPa, the intensity of Raman mode near 150 $cm^{-1}$ declined quickly, suggesting that PbSe started to go back to the B1 phase. (c) Raman peaks under compression. (d) Raman peaks under decompression.

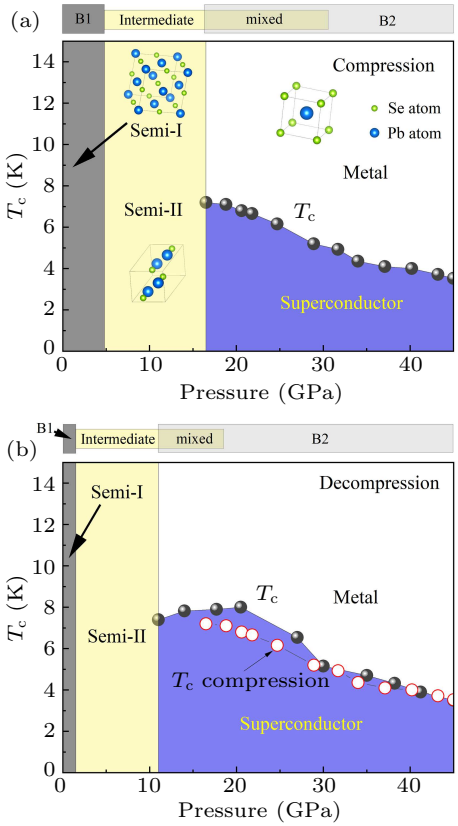



**Fig. 6.** High pressure phase diagrams for PbSe. (a) Phase diagram during the compression process, insets: atomic structure for each phase. (b) Phase diagram during the decompression process. A high $T_c = 8.0$ K is achieved at 20.0 GPa. The Semi-I means the NaCl-type semiconducting phase (B1 phase). Semi-II is the intermediate semiconducting phase. B2 means the CsCl-type structure. Mixed means the coexistence of the intermediate phase and the B2 phase. Upper panel colors: gery represents the B1 phase, yellow represents the intermediate phase, light gery represents the B2 phase.

Based on the experimental findings of the electrical transport measurement and Raman spectra of PbSe under pressure, we proposed phase diagrams for both compression and decompression processes, as seen in Fig. 6. During the compression process, as shown in Fig. 6(a), PbSe is in the B1 phase as a narrow band gap semiconductor below 4.8 GPa, referred to as Semi-I. As the pressure increases to 4.8 GPa, an intermediate *Pnma* phase emerges, leading to a more insulating state, referred to as Semi-II. With further compression, the conductivity of the intermediate phase increases continuously and eventually causes a transition from the semiconducting intermediate phase to the metallic B2 phase at 16.5 GPa, as indicated by transport measurement in Fig. 2. At the same time, PbSe exhibits superconductivity at low temperatures. The intermediate phase and the B2 phase coexist until 30.5 GPa, which is indicated by the evolution of Raman peaks. We refer to the range from 16.5 GPa to 30.5 GPa as the mixed phase (intermediate + B2 Phase). Above 30.5 GPa, PbSe is in pure B2 phase. For superconductivity, $T_c$ decreases monotonously, and the SC phase persists at least to 45 GPa, the highest pressure in this experiment. During decompression, PbSe reenters the mixed phase from the B2 phase below 18.6 GPa. A higher critical temperature ($T_c = 8.0$ K) is observed at 20.5 GPa. The critical pressures for the two structural phase transitions shift to lower values, as shown in Fig. 6(b).

A higher $T_c$ value of 8 K observed during decompression process is due to the fact that the superconductivity with such a $T_c$ is presented in a pure B2 phase rather than the mixed

phase, as the superconductivity will be affected by the structural instability or lattice distortion in the mixed phase. Earlier studies have claimed that there is a Peierls-like lattice distortion during the transition from the B1 phase to the intermediate phase.[46,47] As pressure increases, this lattice distortion is suppressed when the B2 phase appears, and then the superconductivity occurs. During the decompression process, this lattice distortion is recovered when the pressure is released to $\sim$ 17.6 GPa as indicated by the active Raman signal of the intermediate phase in Fig. 5(b). When the pressure was released from 17.6 GPa to 11.0 GPa, more and more intermediate phase would recover from the B2 phase, and the superconductivity was then affected by the structural instability or the lattice distortion, which resulted in a decreasing trend of $T_c$ values. However, during the compression process, the mixed phase started from 16.5 GPa and persisted to 30.5 GPa, as seen in Figs. 2 and 6(a). Then, it is easy to understand why the $T_c$ values are always lower from 16.5 GPa to 30.5 GPa during compression process than those during the decompression process.

## 4. Conclusion

To summarize, we conducted a study on the electrical transport properties of PbSe under pressure. We found that the superconductivity initiated at as early as 16.5 GPa when PbSe just transformed to the B2 phase, and it showed a $T_c$ of 7.2 K. More importantly, the superconductivity ($T_c$) in pure PbSe shows a typical negative pressure dependence. Such a trend is well consistent with its sister compounds PbS and PbTe and is totally different from previous positive pressure dependence. A high $T_c = 8$ K was observed at 20.5 GPa during the decompression process, which is the highest record in all derivatives of PbSe. This research clarifies the misconceptions and provides valuable insights into the intrinsic superconductivity of PbSe, thereby contributing to the understanding of the superconductivity mechanism in lead chalcogenide-based systems.

## Acknowledgements

This work was supported by the National Natural Science Foundation of China (Grant Nos. 12374050, 12004014, U1930401, and 12375304), the National Key R&D Program of China (Grant Nos. 2021YFA1400300 and 2023YFA1608900), and the Major Program of the National Natural Science Foundation of China (Grant No. 22090041). Part of the experimental work was carried out at the Synergetic Extreme Condition User Facility (SECUF, https://cstr.cn/31123.02.SECUF).

## References

[1] Chen Z W, Ge B H, Li W, Lin S Q, Shen J W, Chang Y J, Hanus R, Snyder G J and Pei Y Z 2017 *Nat. Commun.* **8** 13828
[2] Sun J C, Zhang Y, Fan Y T, Tang X F and Tan G J 2022 *J. Chem. Eng.* **431** 133699
[3] Biswas K, He J, Blum I D, Wu C I, Hogan T P, Seidman D N, Dravid V P and Kanatzidis M G 2012 *Nature* **489** 414
[4] Li J F, Liu W S, Zhao L D and Zhou M 2010 *NPG Asia Mater.* **2** 152
[5] Ekuma C E, Singh D J, Moreno J and Jarrell M 2012 *Phys. Rev. B* **85** 085205
[6] Zemel J N, Jensen J D and Schoolar R B 1965 *Phys. Rev.* **140** A330
[7] Phuphachong T, Assaf B A, Volobuev V V, Bauer G, Springholz G, De Vaulchier L A and Guldner Y 2017 *Crystals* **7** 29
[8] Aminorroaya Yamini S, Patterson V and Santos R 2017 *ACS Omega* **2** 3417
[9] Wrasse E O and Schmidt T M 2014 *Nano Lett.* **14** 5717
[10] Kim Y, Kane C, Mele E and Rappe A M 2015 *Phys. Rev. Lett.* **115** 086802
[11] Barone P, Rauch T C V, Di Sante D, Henk J, Mertig I and Picozzi S 2013 *Phys. Rev. B* **88** 045207
[12] Liang T, Gibson Q, Xiong J, Hirschberger M, Koduvayur S P, Cava R J and Ong N P 2013 *Nat. Commun.* **4** 2696
[13] Liang T, Kushwaha S, Kim J, Gibson Q, Lin J, Kioussis N, Cava R J and Ong N P 2017 *Sci. Adv.* **3** e1602510
[14] Matsushita Y, Wianecki P A, Sommer A T, Geballe T H and Fisher I R 2006 *Phys. Rev. B* **74** 134512
[15] Fogel N Y, Buchstab E I, Bomze Y V, Yuzephovich O I, Mikhailov M Y, Sipatov A Y, Pashitskii E A, Shekhter R I and Jonson M 2006 *Phys. Rev. B* **73** 161306
[16] Fogel N Y, Buchstab E I, Bomze Y V, Yuzephovich O I, Sipatov A Y, Pashitskii E A, Danilov A, Langer V, Shekhter R I and Jonson M 2002 *Phys. Rev. B* **66** 174513
[17] Agassi D and Chu T K 1990 *Phys. Stat. Sol. (b)* **160** 601
[18] Fogel N Y, Pokhila A S, Bomze Y V, Sipatov A Y, Fedorenko A I and Shekhter R I 2001 *Phys. Rev. Lett.* **86** 512
[19] Ovsyannikov S V, Shchennikov V V, Manakov A Y, Likhacheva A Y, Ponosov Y S, Mogilenskikh V E, Vokhmyanin A P, Ancharov A I and Skipetrov E P 2009 *Phys. Stat. Sol. (b)* **246** 615
[20] Wang S M, Zang C P, Wang Y K, Wang L P, Zhang J Z, Childs C, Ge H, Xu H W, Chen H Y, He D W and Zhao Y S 2015 *Inorg. Chem.* **54** 4981
[21] Chattopadhyay T, Werner A, Von Schnering H G and Pannetier J 1984 *Rev. Phys. Appl.* **19** 807
[22] Ovsyannikov S V, Shchennikov V V, Manakov A Y, Likhacheva A Y, Berger I F, Ancharov A I and Sheromov M A 2007 *Phys. Stat. Sol. (b)* **244** 279
[23] Chattopadhyay T, Von Schnering H G, Grosshans W A and Holzapfel W B 1986 *Physica B&C* **139** 356
[24] Rousse G, Klotz S, Saitta A M, Rodriguez-Carvajal J, McMahon M I, Couzinet B and Mezouar M 2005 *Phys. Rev. B* **71** 224116
[25] Bencherif Y, Boukra A, Zaoui A and Ferhat M 2011 *Mater. Chem. Phys.* **126** 707
[26] Fujii Y, Kitamura K, Onodera A and Yamada Y 1984 *Solid State Commun.* **49** 135
[27] Li Y, Lin C, Li H, Li X and Liu J 2013 *High Pressure Res.* **33** 713
[28] Li Y, Li G, Lin C, Li X and Liu J 2014 *J. Appl. Phys.* **116** 053502
[29] Li Y, Lin C, Xu J, Li G, Li X and Liu J 2014 *AIP Adv.* **4** 127112
[30] Zhang H, Zhong W, Meng Y H, Yue B B, Yu X H, Wang J T and Hong F 2023 *Phys. Rev. B* **107** 174502
[31] Brandt N B, Gitsu D V, Popovich N S, Sidorov V I and Chudinov S M 1975 *JETP Lett.* **22** 104
[32] Chen L C, Chen P Q, Li W J, Zhang Q, Struzhkin V V, Goncharov A F, Ren Z and Chen X J 2021 *Phys. Rev. B* **103** 214516
[33] Chen L C, Yu H, Wang X Y, Zhang Q, Struzhkin V V and Chen X J 2022 *Phys. Rev. B* **105** 174503
[34] Zolotavin P and Guyot-Sionnest P 2012 *ACS Nano* **6** 8094
[35] Yuzephovich O I, Mikhailov M Y, Bengus S V, Aladyshkin A Y, Pestov E, Nozdrin Y N, Sipatov A Y, Buchstab E and Fogel N Y 2008 *Low Temp. Phys.* **34** 985
[36] Pei C Y, Zhu P, Li B T, Zhao Y, Gao L L, Li C H, Zhu S H, Zhang Q H, Ying T P, Gu L, Gao B, Gou H Y, Yao Y S, Sun J, Liu H Y, Chen Y L, Wang Z W, Yao Y G and Qi Y P 2023 *Sci. China Mater.* **66** 2822

[37] Song C L, Ma X C and Xue Q K. 2020 *MRS Bull.* **45** 366

[38] Hong F, Yang L X, Shan P F, Yang P T, Liu Z Y, Sun J P, Yin Y Y, Yu X H, Cheng J G and Zhao Z X 2020 *Chin. Phys. Lett.* **37** 107401

[39] Yue B B, Zhong W, Deng W, Wen T, Wang Y G, Yin Y Y, Shan P F, Wang J T, Yu X H and Hong F 2023 *J. Am. Chem. Soc.* **145** 1301

[40] Hong F, Shan P F, Yang L X, Yue B B, Yang P T, Liu Z Y, Sun J P, Dai J H, Yu H, Yin Y Y, Yu X H, Cheng J G and Zhao Z X 2022 *Mater. Today Phys.* **22** 100596

[41] Mao H K, Xu J A and Bell P M 1986 *J. Geophys. Res.: Solid Earth* **91** 4673

[42] Allgaier R S and Scanlon W W 1958 *Phys. Rev.* **111** 1029

[43] Jiang Y Y, Pei C Y, Wang Q, Wu J F, Zhang L L, Xiong C and Qi Y P 2024 *Chin. Phys. B* **33** 126105

[44] Gurevich A 2003 *Phys. Rev. B* **67** 184515

[45] Ovsyannikov S V, Ponosov Y S, Shchennikov V V and Mogilenskikh V E. 2004 *Phys. Stat. Sol. (c)* **1** 3110

[46] Shchennikov V, Ovsyannikov S and Derevskov A Y 2002 *Phys. Solid State* **44** 1845

[47] Ovsyannikov S V, Shchennikov V V, Popova S V and Derevskov A Y 2003 *Phys. Stat. Sol. (b)* **235** 521